Cooperative Phenomena in Artificial Solids Made from Silver Quantum Dots: The Importance of Classical Coupling

J. J. Shiang and J. R. Heath*

Department of Chemistry and Biochemistry, University of California, Los Angeles, Los Angeles, California 90095

C. P. Collier and R. J. Saykally

Department of Chemistry, University of California, Berkeley, Berkeley, California 94720

Received: February 26, 1998

Recent work has shown that metal quantum dots can be treated as "artificial atoms" and crystallized into "artificial solids" that have electronic properties that can be tuned by controlling interparticle coupling through the application of pressure. The interactions between the nanocrystals in such artificial solids are classified as either dipole or exchange.[1] Dipole (including many-body) coupling between nanocrystals is treated in a classical manner using an effective medium model that permits the calculation of both the linear and nonlinear optical spectra of the solid as the interparticle separation is continuously varied. We find agreement between the classical model and experimental linear reflectance data until the crystallites are separated by less than 10 Å, after which they sharply diverge. We find that the classical model fails to predict the overall experimental trend in second-harmonic intensities.

Introduction

In an extended crystal the interactions between atoms or molecules can be divided into two broad categories, exchange and dipole. The magnitude and directionality of these interactions determine the band structure of the solid. Which mechanism is operative depends upon the distance between the constituent atoms or molecules. Exchange interactions, where electrons are shared between sites, are important when the atoms/molecules are in close proximity, i.e. a few angstroms. The interactions between the dipole moments of atoms and molecules are much longer range. The different interactions also sample different parts of the electronic wave functions on each atom or molecule. Exchange interactions sample most strongly the outer reaches of the wave functions, whereas dipole interactions depend upon the properties of the entire wave function. An alternative perspective on these interactions is to note that dipole−dipole interactions are basically classical: once the atomic or molecular wave function is known, then they are fully determined via classical electrodynamics. Exchange interactions, on the other hand, are fully quantum in nature. Thus, as a function of interatomic or molecular separation, the band structure of a solid is either "classical" or "quantum" in nature.

Recent advances in quantum dot synthesis[2,3] have made it possible to prepare narrow size distributions of a variety of nanocrystals. For narrowest particle size distributions ($<\sim$5%), various groups have been able to crystallize metal[4−9] and semiconductor[10−12] quantum dots (QDs) into ordered superlattice structures. This work has raised the possibility of fabricating solids that have a tunable electronic band structure. In such a material, the particles would behave as "atoms", and the bulk electronic structure would be determined by the single-particle electronic wave functions and the distance between the crystallites, thus permitting the band structure of a solid to be tuned between the "classical" (dipole) and the "quantum" (exchange) regimes at will. In practice, however, such tunability has been difficult to achieve, and only classical interactions have been reported for semiconductor QDs.[13] For certain metal QD systems, we have recently reported that strong quantum interactions can be observed when the interparticle separations in ordered monolayers become less than $\sim$1 nm.[14] In that work, we utilized a Langmuir trough to compress ordered monolayer films of organically functionalized silver quantum dots. We measured the linear and nonlinear optical properties of the monolayers as a continuous function of interparticle separation, from $D/2r = 1.7$ to <1.1. Here, D is the distance between the centers of adjacent particles, and $2r$ is the diameter of the metal core of a single particle. In the range $D/2r = 1.7-1.2$, we reported evidence of both quantum and classical interparticle coupling. Below $D/2r = 1.2$ ($<5 \pm 2$ Å interparticle separation distance), we observed a *reversible* insulator to metal transition. In this article, we model the behavior of a monolayer composed of alkanethiol-coated, 30 Å diameter, silver crystallites as continuously decreasing functions of interparticle separation. Such a calculation permits us to better discriminate between the "classical" and "quantum" regions of the electronic behavior of the superlattice. We calculate the effect of interparticle separation distance on reflectivity, absorptivity, surface plasmon resonance (ω_{sp}) line width, and nonlinear optical response ($\chi^{(2)}$). We find that the classical approximations reproduce many of the linear optical properties only for $D/2r > 1.25$, such as the position and intensity of the primary surface plasmon resonance and the overall trends in line shape. However, the classical calculations do not reproduce the $D/2r$ dependence of $\chi^{(2)}$.

* Author to whom correspondence should be addressed. E-mail: heath@chem.ucla.edu.

S1089-5647(98)01315-7 CCC: $15.00
Published on Web 04/09/1998

Below $D/2r = 1.2$, all experimental observations strongly diverge from the classical predictions.

Among the earliest classical calculations of the total dielectric response of such assemblies is the Maxwell−Garnett (MG) theory, which has a particularly simple derivation.[15] The Maxwell−Garnett equation relates the total dielectric response of an assembly of spheres embedded in a dielectric to the number density of the spheres and the single-sphere polarizability. The single-sphere polarizability is readily computed using the Clausius−Mossotti (Lorenz−Lorentz) equation.[16] MG theory had originally been formulated for relatively dilute systems with low volume filling factors. Various approaches to mathematically quantifying high multibody interactions between metallic particles in more dense colloids have been developed, dating back to the very early work of Lord Rayleigh.[17] One approach, developed by Torquato and Lado,[18] and further implemented by Farbman and co-workers[19] (and referred to by them as the TKF model), has a straightforward formulation, and we use it here.[20,21] Once the dielectric response of the assembly is found, we can use it to calculate the reflectivity and absorbance of the film. Finally, we can calculate the local field enhancement around a nanoparticle, thus obtaining a classical estimate of the resulting enhancement in $\chi^{(2)}$ versus nanoparticle separation.

Results and Discussion

Polarizability of a Single Crystallite. The frequency-dependent polarizability of a single, isolated Ag crystallite may be calculated from the experimentally determined dielectric response of bulk silver, an estimate of the electronic relaxation time, and the Clausius−Mossotti equation. First, we define the following parameters: $v_f = 1.4 \times 10^8$ cm s^{-1} is the Fermi velocity in bulk Ag; $l = 57 \times 10^{-7}$ cm is the mean free path of an electron in bulk silver; $\omega_p = 1.39 \times 10^{16}$ s^{-1} is the (free electron) bulk plasmon frequency; $\omega_{ci} = v_f/l$ is the collision rate of electrons in the bulk (equal to the bulk plasmon line width).

The Drude model for the dielectric constant of the bulk is

$$\epsilon_{D,b} = \left(1 - \frac{{\omega_p}^2}{{\omega_{ci}}^2 + \omega^2}\right) + \frac{i{\omega_p}^2\omega_{ci}}{\omega({\omega_{ci}}^2 + \omega^2)} \quad (1)$$

The line width due to finite size is

$$\omega_c(r) = \left(\frac{1}{l} + \frac{1}{r}\right)v_f \quad (2)$$

Equations 1 and 2 combine to give the Drude model for a finite size crystal:

$$\epsilon_{D,f}(\omega, r) = \left(1 - \frac{{\omega_p}^2}{{\omega_c}^2(r) + \omega^2}\right) + \frac{i{\omega_p}^2\omega_c(r)}{\omega({\omega_c}^2(r) + \omega^2)} \quad (3)$$

We calculate ϵ_p as the experimental (bulk) dielectric minus the Drude model (bulk) dielectric plus the finite size Drude model. ϵ_p may be thought of as an experimentally determined correction to the bulk Drude model, scaled for finite size. If the bulk dielectric was the true Drude model, the sum of the first two terms would be 0:

$$\epsilon_p(\omega, r) = (\omega_{exp,b}(\omega) - \epsilon_{D,b}(\omega)) + \epsilon_{D,f}(\omega, r) \quad (4)$$

Here, $\epsilon_{exp,b}(\omega)$ is the experimentally determined bulk complex dielectric function. Real and imaginary values for $\epsilon_{exp,b}(\omega)$ were taken from a published reference[22] and interpolated where necessary. $\beta(\omega, r)$ is the Clausius−Mossotti result for the polarizability of a sphere (proportional to r^3). For a sphere with radius r embedded in hexane, it is[16]

$$\beta(\omega, r) = \frac{\epsilon_p(\omega, r) - \epsilon_m}{\epsilon_p(\omega, r) + 2\epsilon_m} \quad (5)$$

Here, ϵ_m is the dielectric constant of hexane ($\epsilon_m = 1.9$). The value of 1.9 is typical of hydrocarbon compounds, and its use reflects the alkylthiol used to stabilize the crystallites. In addition, the presence of the hydrocarbon surfactant partially isolates the crystallites from the substrate (water $\epsilon = 1.74$). This minimizes the effects of anisotropy in the effective medium.

Dielectric Response and Optical Properties of the Assembly of Crystallites. The effective dielectric constant of a two-dimensional two-phase composite medium consisting of spherical metal particles with a defined radius r_0, uniformly dispersed in a continuous phase of dielectric constant ϵ_m, is given by

$$\epsilon_{eff}(\omega, \phi) = \frac{1 + \phi\beta(\omega, r_0) - (1 - \phi)\beta^2(\omega, r_0)\,\zeta(\phi)}{1 - \phi\beta(\omega, r_0) - (1 - \phi)\beta^2(\omega, r_0)\,\zeta(\phi)}\epsilon_m(\omega) \quad (6)$$

In eq 6, ϕ is the packing fraction. $\zeta(\phi)$ is a structure parameter calculated by Milton[23] and Torquato and Lado,[18] and it represents the three-body coupling between all the different spheres that are characterized by a polarizability $\beta(\omega)$. ζ has a strong ϕ dependence, ranging from 0 in the limit of an infinitely dilute dispersion to values approaching unity for closely packed systems. Thus, eq 6 approaches the Maxwell−Garnett expression for dipolar coupling for small values of ϕ. For three-dimensional dispersions, tabulated ζ as a function of packing density is known for randomly ordered spheres,[18] in addition to the case of fcc-packed spheres.[23] For these two cases, ζ depends upon the degree of order: for a given value of ϕ, ζ is much larger for a randomly packed system than for the fcc-ordered system. In fact, over a wide range of ϕ, ζ for a fcc structure is sufficiently small that eq 6 yields results very similar to the Maxwell−Garnett equation. In a simulation of a randomly packed case, ζ does not change significantly upon reduction from three to two dimensions, and thus we use the 3-D values of ζ in our 2-D model. We can relate ϕ, the packing fraction, to $D/2r$ for the close packed ordered system using

$$\frac{D}{2r} = \left(\frac{\pi}{2\sqrt{3}\phi}\right)^{1/2} \quad (7)$$

For the disordered system we use the tabulated results found in Torquato.[24]

Once the complex dielectric function of the Ag nanocrystals, at some packing fraction ϕ, is known, we can then calculate the reflectivity and absorbance of a monolayer of Ag particles supported on a water surface. We use the formulation found in Heavens for a single absorbing layer on a transparent substrate.[25] The reflectance (the ratio of reflected power to input power) is given by $|R|^2$, where R is given by

$$R = \frac{r_1 + r_2\, e^{-2i\delta}}{1 + r_1\, r_2\, e^{-2i\delta}} \quad (8)$$

and δ is

$$\delta = \frac{2\pi}{\lambda} n \, d \cos(\varphi) \tag{9}$$

λ is the wavelength of the incident light, φ is the angle of incidence, and r_1 and r_2 are the Fresnel reflection coefficients for the air−monolayer (1) and the monolayer−water (2) interfaces. To evaluate r_1 and r_2 we need the complex dielectric constant of the thin film, the film thickness, (i.e., the diameter of a particle), the refractive indices of water (1.34) and air (1.0), and the angle of incidence. We set the incident angle to 0°, which simplifies the calculation considerably and avoids entirely the issue of anisotropy in the medium effective dielectric constant due to the presence of different bounding media. The experimental linear reflectance data presented here were collected 35° from normal; however, one does not expect this difference to seriously impact the overall trends in line position, line width, and local electric field.

The calculated reflectance of a disordered monolayer as a function of interparticle separation is shown in Figure 1. In the calculated reflectance spectra, note the presence of an additional optical transition near 3.25 eV. For a disordered array at low packing fractions, the primary plasmon resonance consists of two convoluted peaks. At higher packing fractions the primary resonance consists of a single peak and a weak shoulder. Figure 2 presents a comparison of the expected peak shift from the solution peak position as a function of $D/2r$ to experiment.[14] Three different models are plotted as lines, and the experimental data are represented by open circles. The error bars emerge from an analysis of TEM micrographs of selected samples. For $D/2r$ values greater than 1.3, a shift of the TKF/disordered calculated result by −0.05 eV would result in close agreement with the experimental data. For 30 Å crystallites, this corresponds to a surface-to-surface separation of the crystallites of 10 Å. The fact that for $D/2r > 1.3$ the data lie between the disordered and ordered curves and have the same overall dependence upon $D/2r$ is consistent with TEM micrographs that show a mostly ordered two-dimensional array of spheres.[14] Below $D/2r$ values of 1.25, the classical model does not reproduce the observed peak shifts.

Figure 3 presents a detailed comparison of the observed and the calculated spectral responses for three different values of $D/2r$. The experimental spectra were referenced to the bare water substrate. For $D/2r = 1.6$, the calculated spectra (given in terms of reflectance) were multiplicatively scaled to match the experimental spectra (given in counts). Overlap of the spectra also required the use of a small constant baseline scaling which accounts for small variations in the experimental baseline reference to the water substrate. To match the peak position, the calculated spectrum was also shifted in energy. The shift is required because there are variations in the absorption maximum of the solution spectrum from sample to sample. The same scaling factor and energy shift from the solution-phase spectrum were applied to the calculated spectrum for $D/2r = 1.38$. The close agreement between model and experiment indicates that the classical model reproduces the trends in intensity, line shape, and peak position of the reflectivity spectra between $D/2r = 1.60$ and 1.38. We applied the same scaling factor, shift from solution spectrum, and baseline offset to the calculation for $D/2r = 1.17$. Unlike the earlier results, there is a large difference in the intensity and position, as well as line shape. We attributed the narrowing of the experimental surface plasmon line width at small interparticle separation to quantum mechanical coupling, where delocalization of charge carriers over multiple particles increases the scattering lifetime.[14,26] The trends with $D/2r$ in intensity, line position, and line shape all indicate that the "classical" region of crystallite−crystallite interaction is only applicable for values of $D/2r > 1.25$.

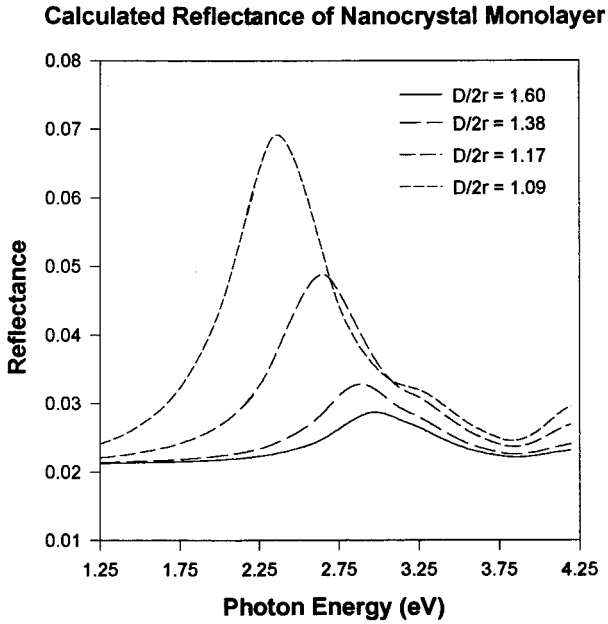

Figure 1. Calculated reflectance spectra for a two-dimensional array of 30 Å Ag crystallites. Spectra were calculated assuming a disordered structure and multibody effects. Spectra corresponding to four different values of the packing fraction are shown.

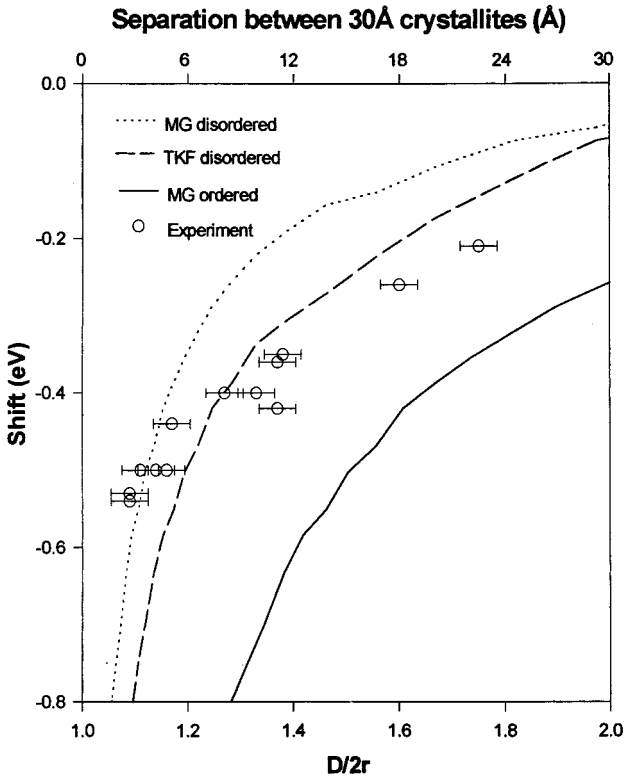

Figure 2. Calculated (lines) and experimental (open circles) results for the shift of the surface plasmon peak from its value in solution. The Maxwell−Garnett (MG) theories for disordered and ordered 2-D superlattices consider dipole coupling only. The TKF model accounts for many-body coupling effects.

Before leaving our discussion of line shape, we also consider the possibility of line narrowing via a mechanism involving energy transfer between particles. As our monolayers are compressed, the primary excitation peak is observed to narrow by between 15 and 30%. In a system of coupled oscillators,

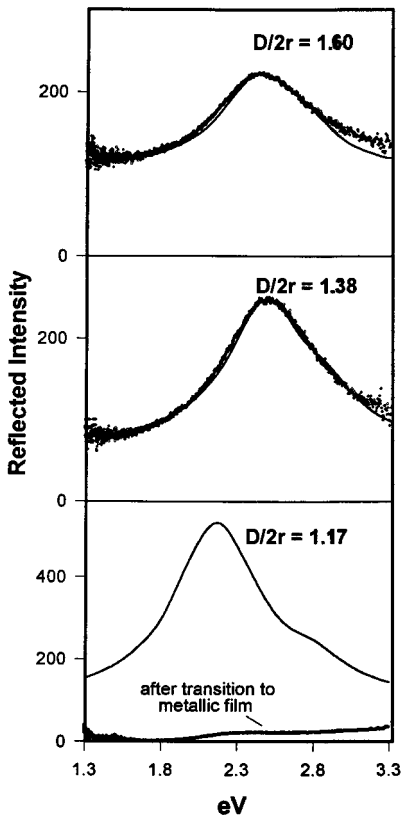

Figure 3. Comparison of calculated and experimental reflectance spectra for three values of $D/2r$. The calculated spectrum for $D/2r = 1.6$ (top, lines) was multiplicatively scaled and shifted in energy to match the experimental spectrum (points). The same scaling and energy shift were applied to the calculated spectra for $D/2r = 1.38$ (middle) and $D/2r = 1.17$ (bottom). The experimentally observed reflectance vs $D/2r$ closely follows the classical approximation until about $D/2r = 1.25$ or so. Below $D/2r = \sim 1.15$, the particle monolayer undergoes a reversible metal insulator transition. The observed reflectance of the metallic phase, shown at the bottom, bears no resemblance to the classical prediction.

excitation of any single oscillator will eventually lead to energy transfer to the other oscillators. Energy transfer can proceed either by exchange or by dipole coupling. Modeling exchange effects requires a detailed knowledge of the wave functions, particularly in the regions outside the crystallite boundary. The magnitude of dipole−dipole coupling is given by μ^2/r^3, where μ is the transition dipole moment, which can be estimated using the Clausius−Mossotti equation. If the excitation is no longer confined to a single site, slowly modulated differences in the site energy, which would normally lead to inhomogeneous broadening, are "averaged" out.[27] Thus, in the case of very weak coupling between the QDs, the absorption maximum is unshifted from its solution value, and its line width reflects both homogeneous (lifetime) and inhomogeneous contributions. In the case of strong coupling between crystallites, the line width contains only lifetime effects. Due to very short lifetime of the plasmon resonance and the relatively weak dependence of the peak position on size, it is unlikely that this mechanism accounts for the observed line narrowing.

To clarify these issues, consider a dimer of two identical particles, each possessing a homogeneously broadened (Lorentzian) plasmon resonance. In this case, as the crystallites are moved closer together and the excitation begins to hop from one site to the other, no change in line width will be observed since both the excitation energy and the lifetime on both sites are the same. It is, in fact, possible to prove mathematically that for a system of two coupled molecules, each of which has a Lorentzian line shape, the absorption line will also have a Lorentzian line shape which has the *same width for all coupling strengths.*[28] Now consider a system in which the crystallites have slightly different absorption maxima, due to a finite size distribution, variations in local chemical environment, etc. When the crystallites are very far apart, the spectrum will consist of two overlapping transitions and will appear to have a width greater than that of a single crystallite. As the interaction between the two sites is turned on, the excitation will transfer rapidly between the two crystallites, and the differences in the site energy will be averaged out. As the coupling strength is increased, the line width will evolve toward a Lorentzian shape with width given by the intrinsic energy transfer lifetime. Extending this argument, the spectrum of a sample in which the crystallites are slightly inhomogeneous will exhibit narrowing as the particle−particle coupling is increased. The ultimate line width, however, is still limited by the intrinsic lifetime of a single crystallite plasmon mode, and thus metal crystallite optical transitions do not undergo the same dramatic *classical* narrowing effects seen in molecular systems such as J-aggregates, which are characterized by much longer lifetimes.

Local Field Effects on SHG Generation. A final experimental result that we presented on Ag quantum dot monolayers is the dependence of the second-order hyperpolarizability ($\chi^{(2)}$) on interparticle separation. We reported that when the particles were compressed from $D/2r = 1.7$ to $D/2r = 1.2$, the optical second-harmonic generation (SHG) increased by a factor of 500, corresponding to a factor of ~22 relative increase in $\chi^{(2)}$. Below $D/2r = 1.2$, the SHG signal sharply decreases to a constant value, independent of any further compression. It is worth noting that $\chi^{(2)}$ samples a different region of the wave function than the linear susceptibility. For $\chi^{(2)}$ to be nonzero, there has to be a perturbation that makes the system non-centrosymmetric. In the monolayers, this condition is met because the dielectric below the monolayer (water) is different from the one above (air). The portion of the metal electron density that is most strongly affected by this perturbation lies outside the boundaries of the crystallite. The reason is simply that electron density between the metallic particles is well shielded from the positive cores[29] and is more susceptible to applied electric or electromagnetic fields. $\chi^{(2)}$ thus samples the same regions of the wave function as the exchange interaction and should be much harder to model using a classical picture.

The increase in $\chi^{(2)}$ can originate from either quantum and/or classical coupling between the particles. Quantum coupling arises from the following picture. If a monolayer of particles is compressed to the point that quantum mechanical wave function overlap between adjacent particles occurs, then electron density will build up in the less shielded region between neighboring metallic cores. This is similar to bringing two hydrogen atoms together to form a chemical bond. Higher order susceptibilities of this electron cloud can then give rise to large increases in nonlinear optical signatures. Since this type of coupling depends upon the overlap between two spatially separated wave functions, the coupling strength should increase exponentially with decreasing interparticle separation. In the classical picture, the mechanism for increased SHG signal with decreasing $D/2r$ is substantially different. In this case, it is the influence of the local electric fields around any given particle that gives rise to large increases in $\chi^{(2)}$, and these local fields arise from dipole and multipole interactions between adjacent particles. In this section, we calculate the frequency-dependent local fields around individual particles as functions of $D/2r$ and

use these results to predict the expected increase in $\chi^{(2)}$ as the particles are compressed.

Computing the local electric field constants at each wavelength relates the internal field (inside a material of dielectric constant ϵ_e) to the external field (i.e., the laser field), from the Lorenz equation[16]

$$E_L(\omega, \phi) = \frac{\epsilon_{eff}(\omega, \phi) + 2}{3} \tag{10}$$

In the experiments, we normalize the SHG signal to some initial value that corresponds to an initial packing fraction of the crystallites when they are first deposited on the Langmuir trough. Here we choose the initial packing fraction to be 0.15, corresponding to $D/2r = 1.7$. We calculate the local field factor[30] and normalize it to the local field factor appropriate for our chosen initial packing fraction. This is the local field enhancement, L, as the particles are compressed together, starting at $D/2r = 1.7$.

$$L = \frac{(E_F(\phi))^2 E_{SH}(\phi)}{(E_F(0.15))^2 E_{SH}(0.15)} \tag{11}$$

Here, E_F and E_{SH} are the frequency-dependent local field factors, taken at the fundamental (ω_f) and second harmonic (ω_{SH}) (1064 nm and 532 nm, respectively). In order to compare directly with experiment, we also need to include the Fresnel factors for our SHG geometry according to the procedure of Mizrahi and Sipe.[31] We then multiply the local field factor with the appropriate Fresnel factor F:[32]

$$L_{Fresnel}(\phi) = \frac{F(\phi) L(\phi)}{F(0.15)} \tag{12}$$

In Figure 4, we present the calculated SHG signal enhancement as a function of $D/2r$, best fit to the function $(D/2r)^{-n}$. The best fit turns out to be for $n \sim 18$, which is the expected result based upon simple dipole−dipole coupling (away from the resonance regime). Also included in Figure 4 are the data from ref 14, along with an exponential fit to the data. Clearly the exponential function is more satisfactory than the local field calculation, implying that the SHG increase is largely arising from quantum mechanical coupling between adjacent particles. Note that, imbedded in this calculation, we have taken into account the fact that the plasmon resonance is shifting throughout the $D/2r$ range of Figure 4.

Conclusions

We have presented a simple classical effective medium calculation of a 2-D monolayer of silver 30 Å diameter nanocrystals and compared it to experimental results. We find that if interparticle separation is greater than about 10 Å, the linear optical response is well described by the classical effective medium model. However, we find that the classical model in no way reproduces the abrupt changes in the reflectance spectrum observed around $D/2r = 1.2$. We also find that the trends in the nonlinear response are not described by the classical model. All of this is consistent with the idea that a fundamental change in the nature of particle−particle interactions, from classical coupling to quantum coupling, occurs when the silver particles are separated by a distance of less that 10 Å. A major challenge is now to extend the description of the collective properties of quantum dot superlattices into this "quantum" regime and thus arrive at a comprehensive description of the development of the electronic band structure in these remarkable materials.

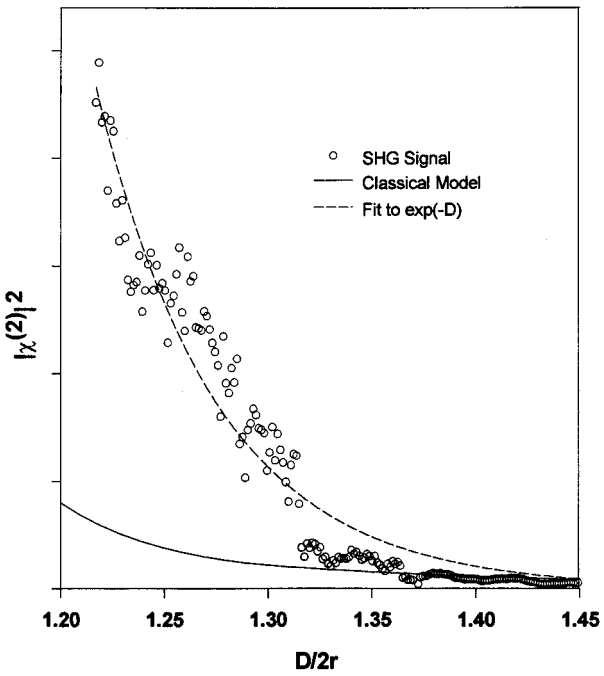

Figure 4. Comparison of second-harmonic signal intensity, $|\chi^{(2)}|^2$, vs $D/2r$. Plotted is the experimental SHG intensity (points), a fit to an exponential function ($A \exp(-B(D/2r))$ (dashed line), and the predictions of the classical model (solid line). The classical model was scaled to match the experimental points at large values of $D/2r$. Note that, similar to the linear optical response, the classical prediction and the experimental observations sharply diverge below a $D/2r$ of about 1.3.

Acknowledgment. This work was supported by the NSF-NYI program. J.R.H. acknowledges support from the Packard Foundation, and a Sloan Fellowship. C.P.C. and R.J.S. acknowledge support from NSF Grant CHE-9424482.

References and Notes

(1) Knox, R. S. *Solid State Physics*; Academic: New York, 1963; Vol. 5.
(2) Murray, C. B.; Norris, D. J.; Bawendi, M. G. *J. Am. Chem. Soc.* **1993**, *115*, 8706.
(3) Brust, M.; et al. *J. Chem. Soc., Chem. Commun.* **1994**, 801.
(4) Ohara, P. C.; Leff, D. V.; Heath, J. R.; Gelbart, W. M. *Phys. Rev. Lett.* **1995**, *75*, 3466.
(5) Whetten, R. L.; et al. *Adv. Mater.* **1996**, *8*, 428.
(6) Andres, R. P.; et al. *Science* **1996**, *273*, 1690.
(7) Griffith Freeman, R.; et al. *Science* **1995**, *267*, 1629.
(8) Grabar, K. C.; et al. *Langmuir* **1996**, *12*, 2353.
(9) Hostetler, M. J.; Green, S. J.; Stokes, J. J.; Murray, R. W. *J. Am. Chem. Soc.* **1996**, *118*, 4212.
(10) Herron, N.; Calabrese; J. C., Farneth, W.; Wang, Y. *Science* **1993**, *259*, 1426.
(11) Vossmeyer, T.; et al. *Science* **1995**, *267*, 1476.
(12) Murray, C. B.; Kagan, C. R.; Bawendi, M. G. *Science* **1995**, *270*, 1335.
(13) (a) Kagan, C. R.; Murray, C. B.; Bawendi, M. G. *Phys. Rev. B* **1996**, *54*, 8633. (b) Kagan, C. R.; Murray, C. B.; Nirmal, M.; Bawendi, M. G. *Phys. Rev. Lett.* **1996**, *76*, 1517.
(14) Collier, C. P.; Saykally, R. J.; Shiang, J. J.; Henrichs, S. E.; Heath, J. R. *Science*, **1997**, *277*, 1978. All experimental data reported in this paper were collected as described in this reference.
(15) Maxwell-Garnett, J. C. *Philos. Trans. R. Soc. London* **1904**, *203*, 385.
(16) Jackson, J. D. *Classical Electrodynamics*, 2d. ed.; John Wiley & Sons: New York, 1975; eqs 4−55 and 4−56.
(17) Raleigh, J. W. S. *Philos. Mag.* **1892**, *34*, 481.
(18) (a) Lado, F.; Torquato, S. *Phys. Rev. B* **1986**, *33*, 3370. (b) Torquato, S.; Lado, F. *Phys. Rev. B* **1986**, *33*, 6428.

(19) Farbman, I.; Levi, O.; Efrima, S. *J. Chem. Phys.* **1992**, *96*, 6477.

(20) An alternative approach would be that of Bagchi, A.; Barrerra, R; Dasgupta, B. *Phys. Rev. Lett.* **1980**, *44*, 1475, which should be valid for a two-dimensional array of crystallites on a dielectric surface. We have evaluated their expressions and found that they give results similar to Maxwell−Garnett.

(21) See: Bosi, G. *J. Opt. Soc. B* **1996**, *13*, 1691, and related papers for alternatives to the effective medium approach.

(22) Landolt-Börnstein. *Numerical Data and Functional Relationships in Science and Technology New Series*; Springer-Verlag: Berlin, 1982; Part III, Vol. 15b.

(23) McPhedron, R. C.; Milton G. W. *Appl Phys. A* **1981**, *26*, 207.

(24) Torquato, S. *Phys. Rev E* **1995**, *51*, 3170.

(25) Heavens, O. S. *Optical Properties of Thin Solid Films*; Butterworths Scientific Publications: London, 1951; Chapter 4.

(26) Heath, J. R.; Leff, D. V.; Knobler, C. M. *J. Phys Chem. B* **1997**, *101*, 189.

(27) (a) Kubo, R. *Adv. Chem. Phys.* **1969**, *15*, 101. (b) Anderson, *J. Phys. Soc. Jpn.* **1954**, *9*, 316.

(28) Hemenger, R. P. *J. Chem. Phys.* **1976**, *66*, 1795.

(29) (a) Kresin, V. *Phys. Rev. B* **1988**, *38*, 3741. (b) Eckardt, W. *Phys. Rev. B* **1985**, *31*, 6360.

(30) Heinz, T. F.; Tom, H. W. K.; Shen, Y. R. *Phys. Rev. A* **1983**, *28*, 1883; last eq.

(31) (a) Lipson, S. G.; Lipson, H.; Tannhauser, D. S. *Optical Physics*, 3rd ed. Cambridge University Press: Cambridge, 1995. (b) Mizrahi, V. Sipe, J. E. *J. Opt. Soc. Am.* **1988**, *5*, 660.

(32) Note added in proof: The Mizrahi and Sipe formulism in ref 31b describes SHG from an infinitely thin polarization sheet at the boundary of two semi-infinite media. However, we have more recently computed the correct Fresnel factors for a film of finite thickness (30 Å) from ref 25 and find that the classical prediction in Figure 4 is essentially unchanged.